Supporting information

Smart Dual T_1 MRI-Optical Imaging Agent Based on Rhodamine Appended Fe(III)-catecholate Complex

Duraiyarasu Maheshwaran,[a] Thavasilingam Nagendraraj,[a] T. Sekar Balaji,[b] Ganesan Kumaresan,[b] S Senthil Kumaran[c] and Ramasamy Mayilmurugan*[a]

[a]Bioinorganic Chemistry Laboratory/Physical Chemistry, School of Chemistry, Madurai Kamaraj University, Madurai 625 021, Tamil Nadu, India.

[b]School of Biological Sciences, Madurai Kamaraj University, Madurai 625 021, Tamil Nadu, India.

[c]Department of NMR, All India Institute of Medical Sciences, Ansari Nagar, New Delhi 110 029, India.

***E-mail:** mayilmurugan.chem@mkuniversity.ac.in

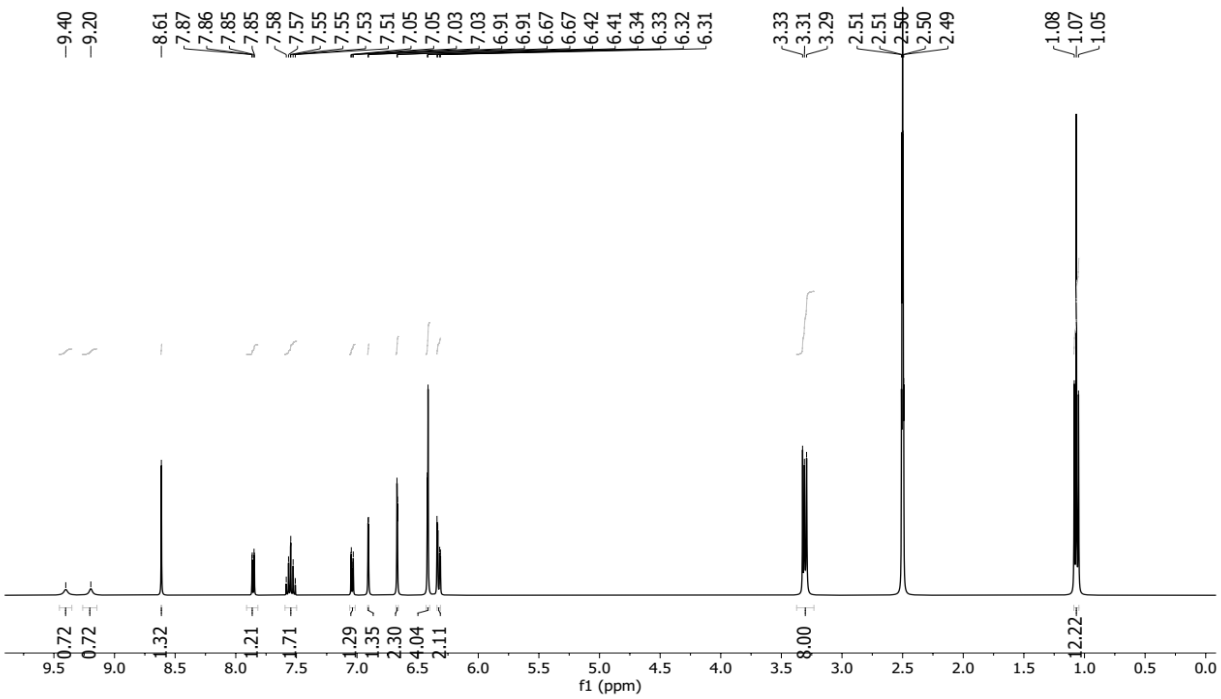

Figure S1. ^{1}H NMR of **RhoCat** in DMSO-d_6.

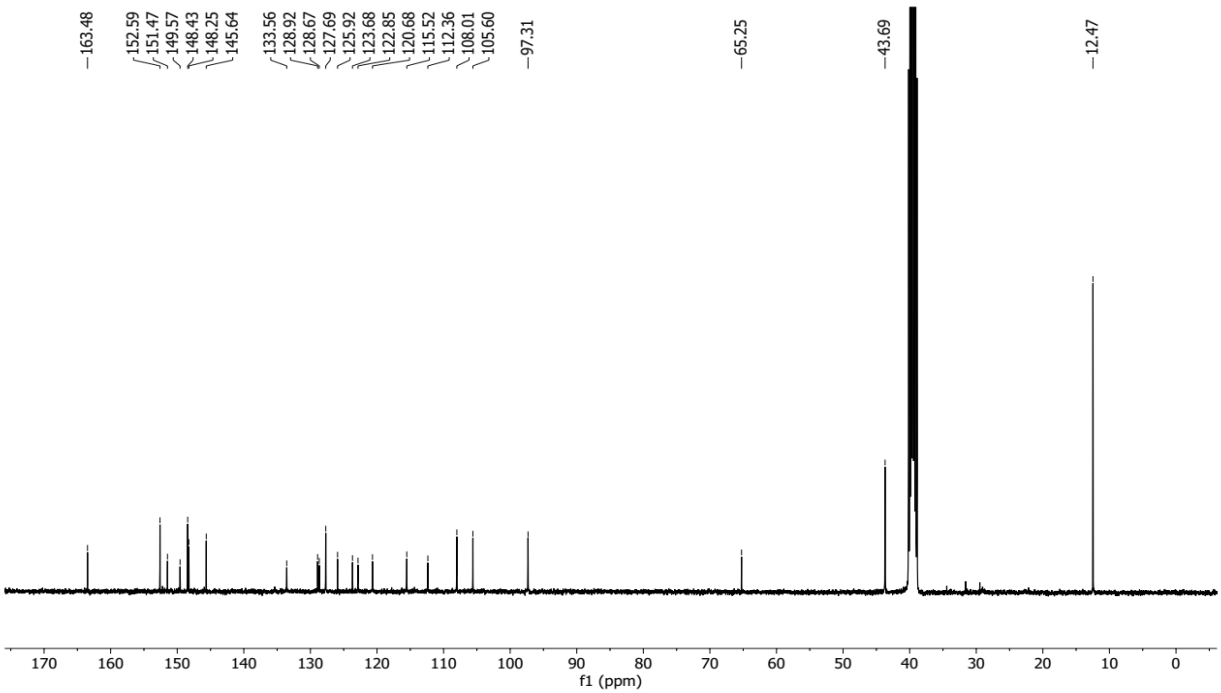

Figure S2. ^{13}C NMR of **RhoCat** in DMSO-d_6.

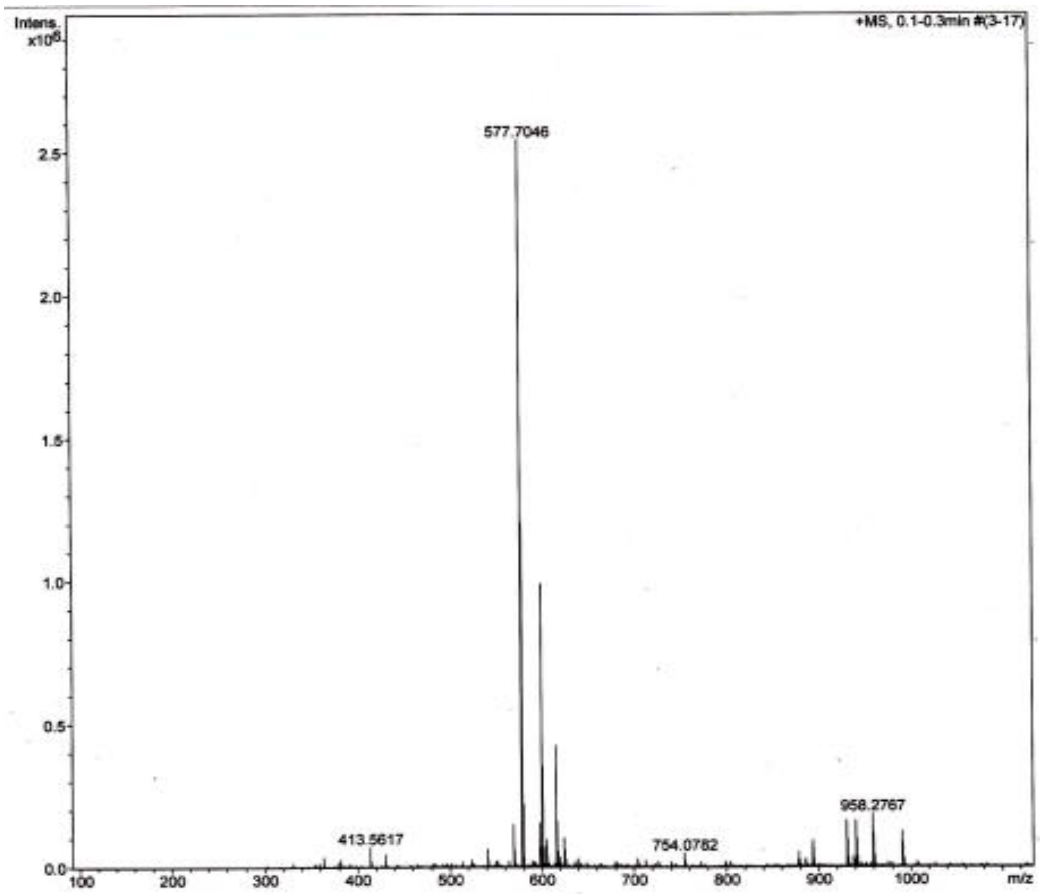

Figure S3. HR-ESI mass spectrum of **RhoCat** in methanol.

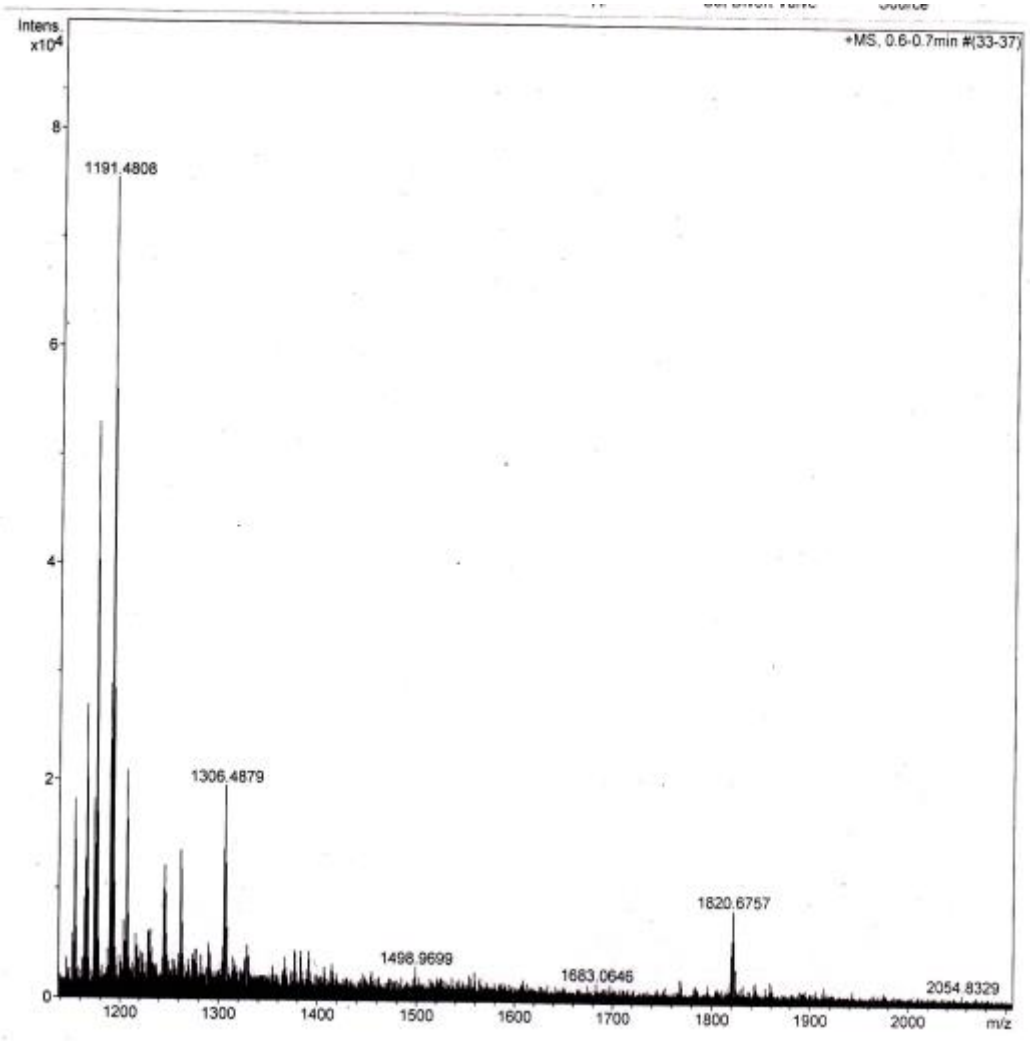

Figure S4. HR-ESI mass spectrum of **Fe(RhoCat)$_3$** in methanol.

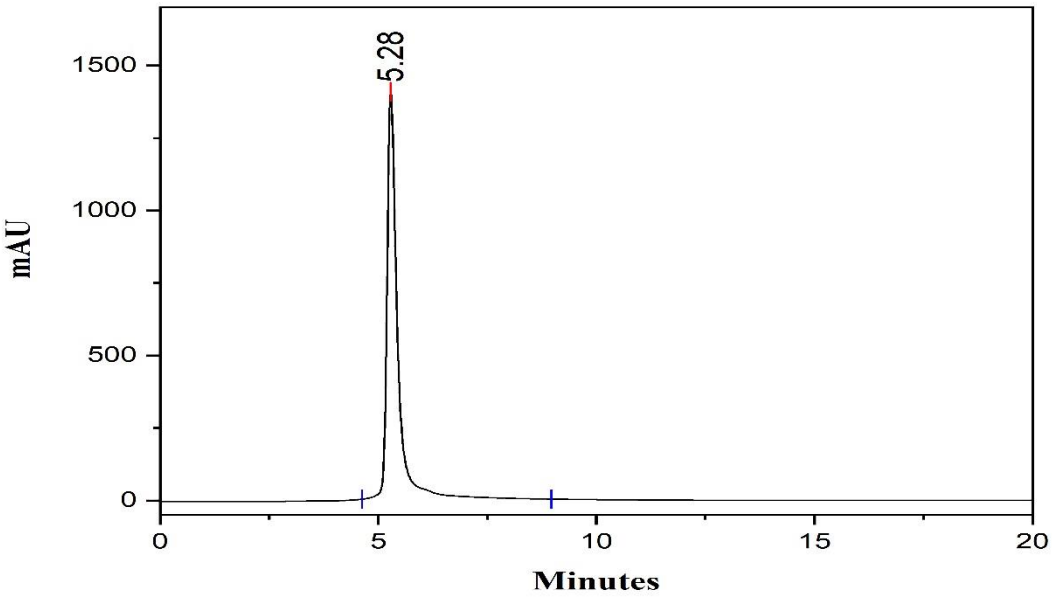

Figure S5. Analytical HPLC chromatogram of **Fe(RhoCat)$_3$** where the absorption at 254 nm indicates the high purity of the sample.

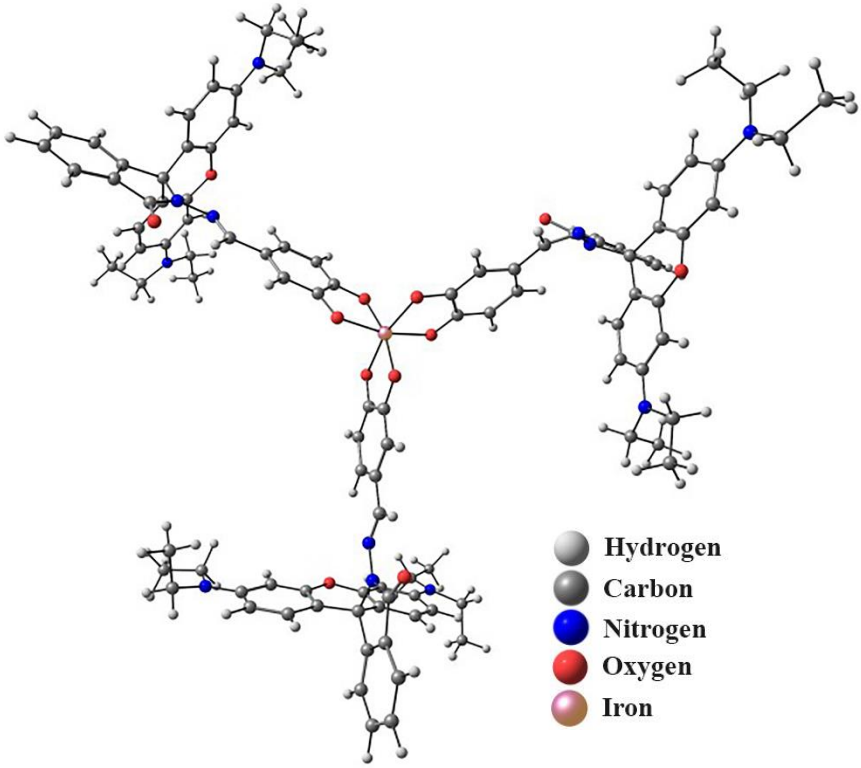

Figure S6. DFT optimized structure of **Fe(RhoCat)$_3$**. Optimized at B3LYP/6-31G(d,p) basis set (for C, H, N and O), LANL2DZ for Fe in Gaussian 16 program.

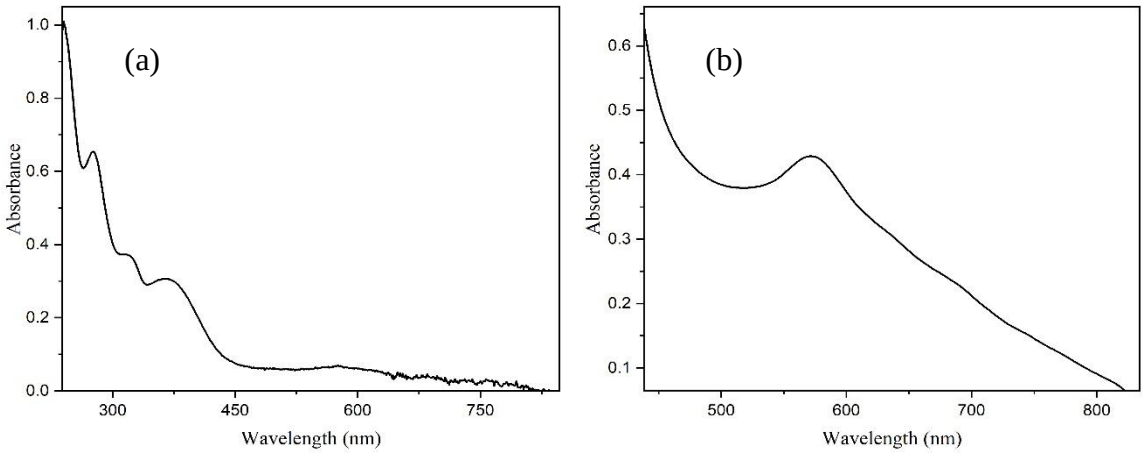

Figure S7. UV/Vis spectrum of **Fe(RhoCat)$_3$** at 40 × 10^{-6} M (a) 2 × 10^{-4} M (b) in phosphate buffer (pH 7.3) at 25 °C.

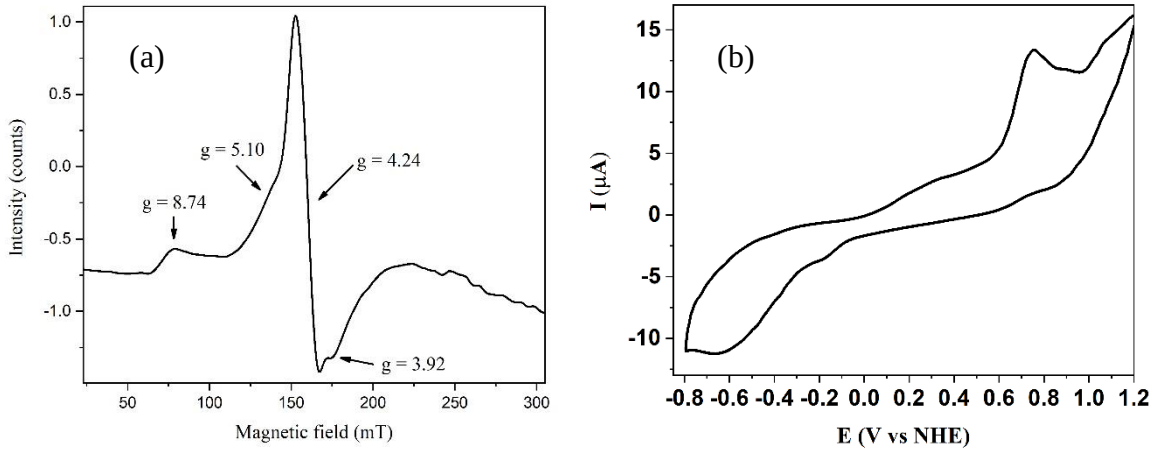

Figure S8. X-band EPR spectrum of **Fe(RhoCat)$_3$** in a methanol/DMF mixture at temperature = 70 K, frequency = 9.5010 GHz, power = 0.7614 mW, modulation amplitude = 4 G, and modulation frequency = 100 kHz (a), Cyclic voltammogram of **Fe(RhoCat)$_3$** (1 × 10^{-3} M) in acetonitrile at 25 °C (reference: saturated Ag/Ag^+; supporting electrolyte: 0.1 M TBAP solution; scan rate: = 100 mV s^{-1}) (b).

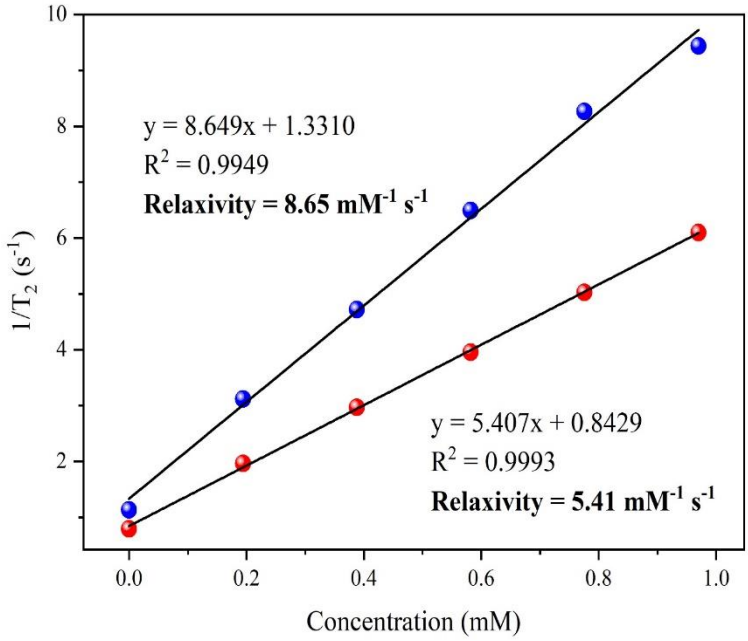

Figure S9. Transverse relaxivity $1/T_2$ versus [Fe(III)] plot of **Fe(RhoCat)$_3$** at 1.41 T, 25 °C in HEPES buffer (pH 7.3) (red spheres) and 4 % BSA solution (blue spheres)

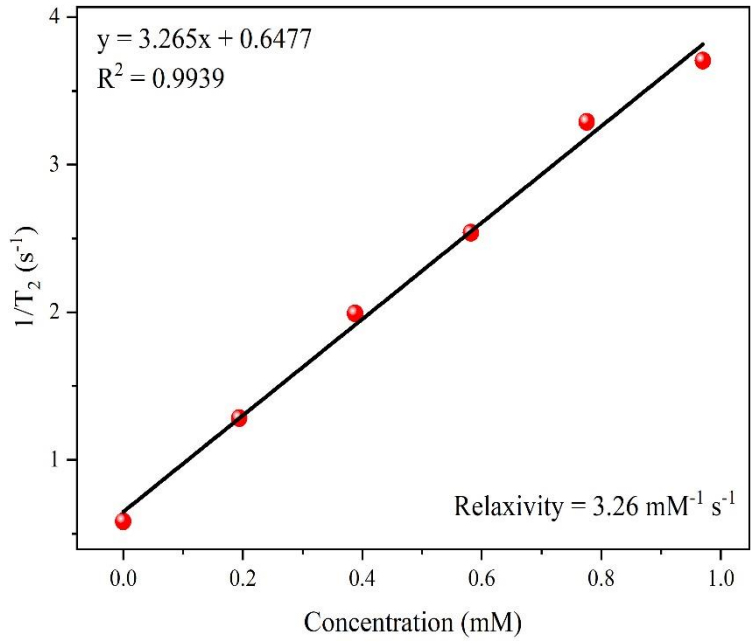

Figure S10. Transverse relaxivity $1/T_2$ versus [Fe(III)] plot of **Fe(RhoCat)$_3$** at 1.41 T, 37 °C in HEPES buffer (pH 7.3).

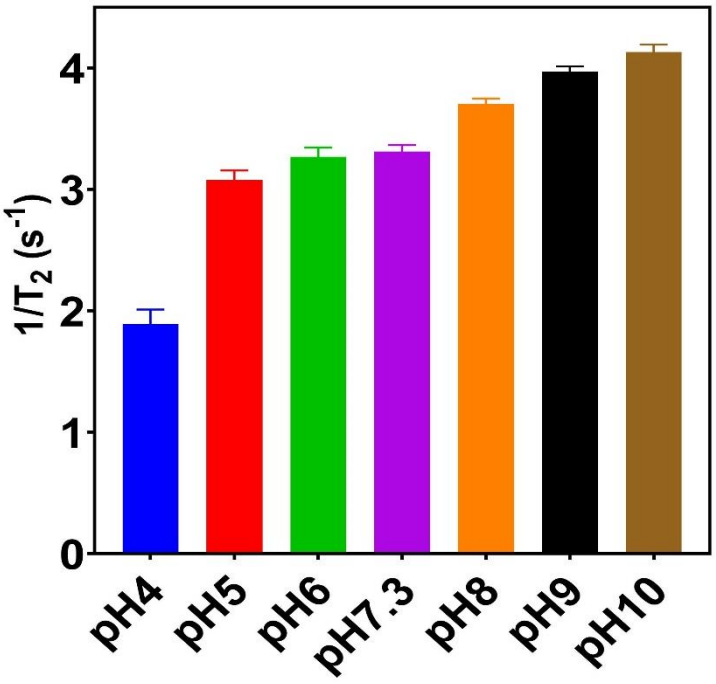

Figure S11. The change in r_2-relaxivity of **Fe(RhoCat)$_3$** versus pH variations (4−10), at 1.41 T, 25 °C and 0.425 mM of Fe(III) concentration.

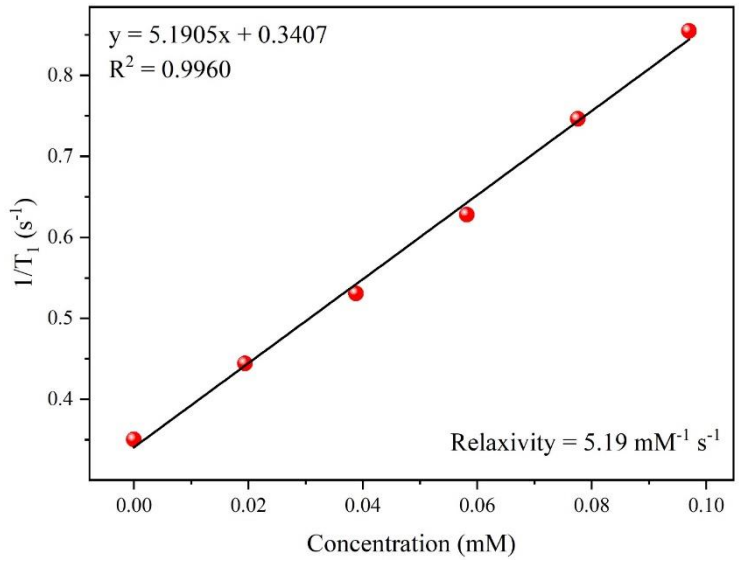

Figure S12. The plot of longitudinal relaxivity $1/T_1$ versus [Fe(III)] for **Fe(RhoCat)$_3$** at 1.41 T, 25 °C in HEPES buffer (pH 7.3) in NO.

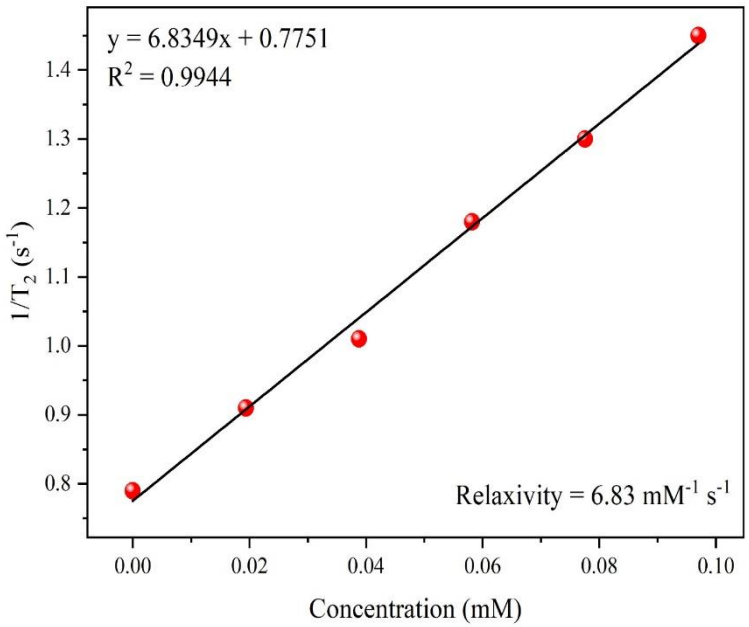

Figure S13. The plot of transverse relaxivity $1/T_2$ versus [Fe(III)] for **Fe(RhoCat)$_3$** at 1.41 T, 25 °C in HEPES buffer (pH 7.3) in NO.

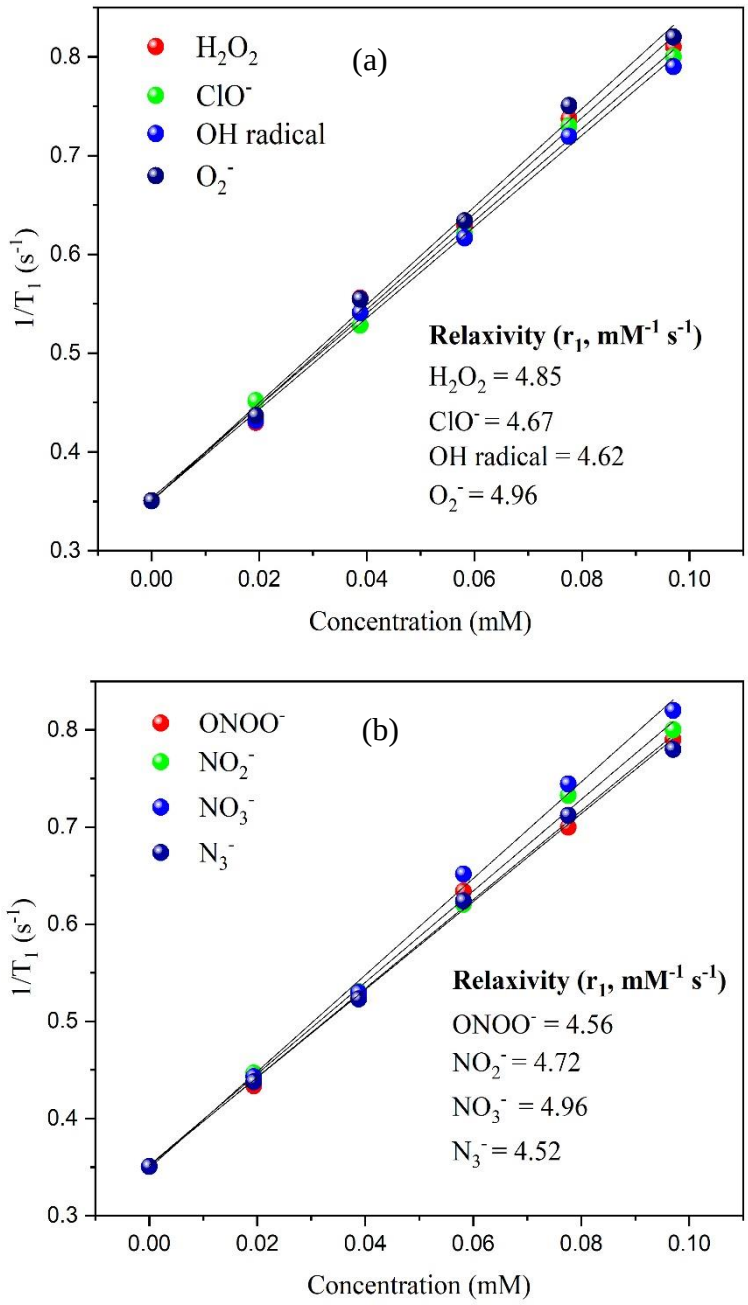

Figure S14. The plot of longitudinal relaxivity $1/T_1$ versus [Fe(III)] for **Fe(RhoCat)$_3$** in ROS (a) and RNS (b) (100 μM) at 1.41 T, 25 °C in HEPES buffer (pH 7.3).

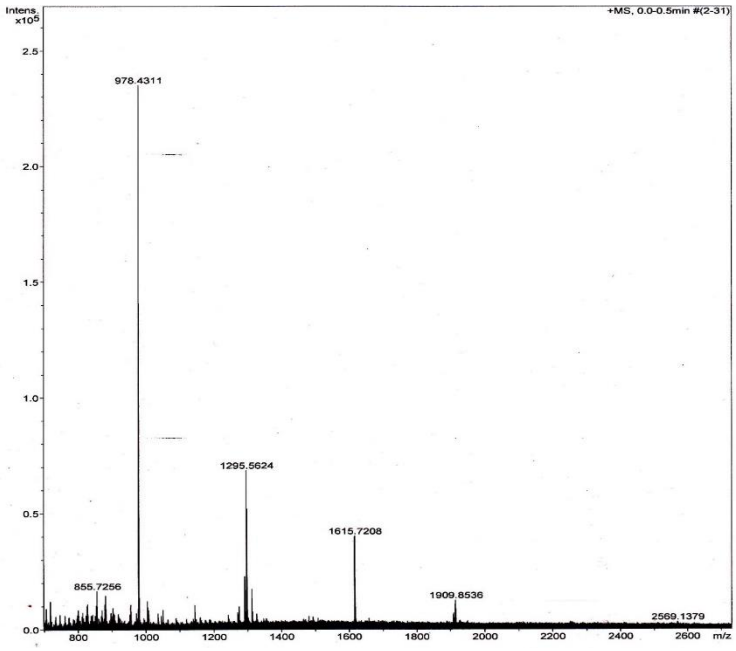

Figure S15. HR mass spectrum of **Fe(NO-RhoCat)$_3$** species in buffer solution**.**

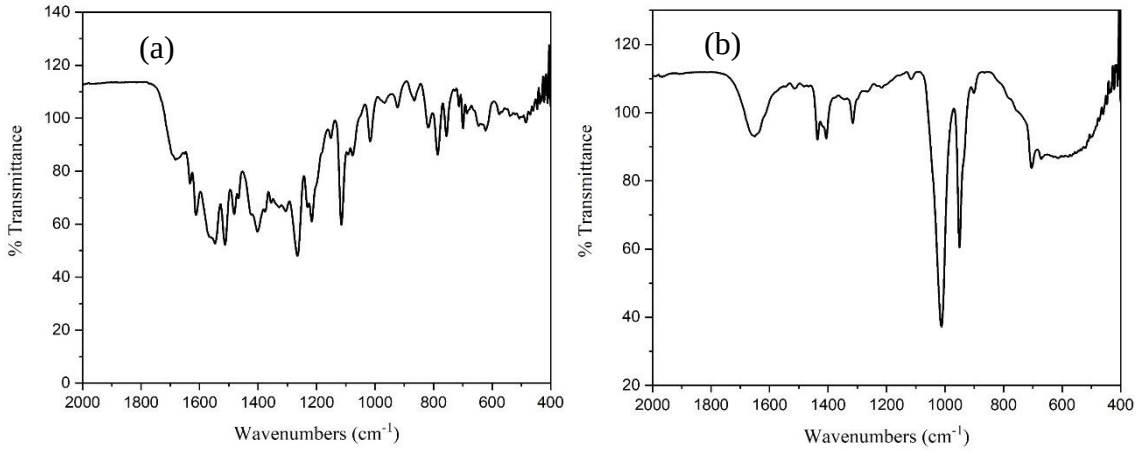

Figure S16. FTIR spectra of **Fe(RhoCat)$_3$** before (a) and after (b) addition of NO.

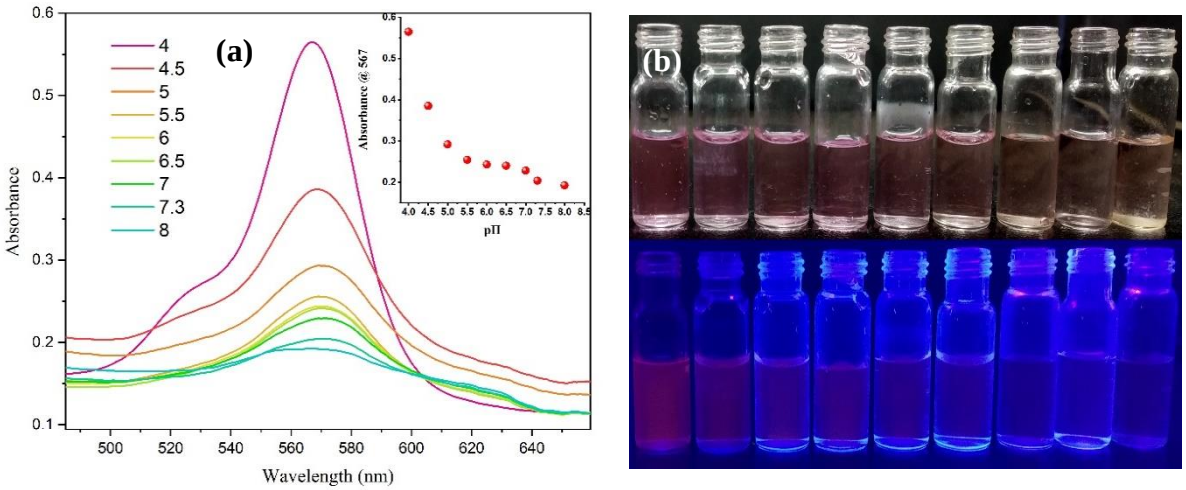

Figure S17. UV-Vis spectral change for **Fe(RhoCat)$_3$** (40 μM) for the pH variation in HEPES buffer solution (a). Inset: plot of absorbance at 567 nm vs pH. Photographs **Fe(RhoCat)$_3$** showing colour change in different pH under visible light (top) and fluorescence changes under UV light (bottom) (b).

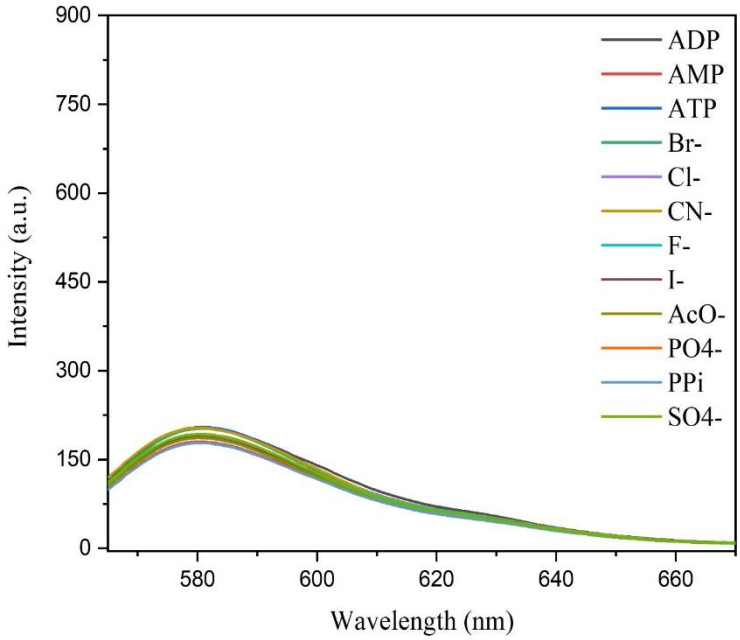

Figure S18. Fluorescence spectra of **Fe(RhoCat)$_3$** (20 μM) with 100 μM anions and phosphates.

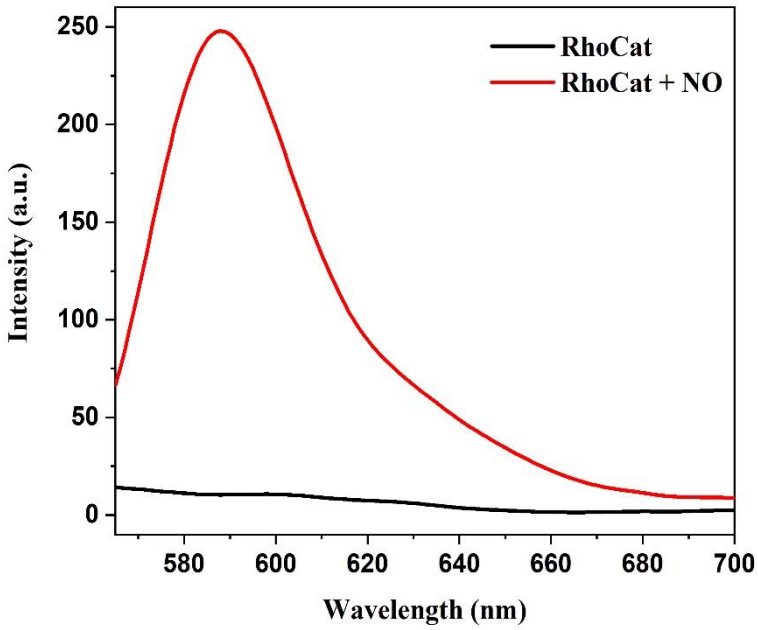

Figure S19. Fluorescence spectra of **RhoCat (**5 μM) with **NO**.

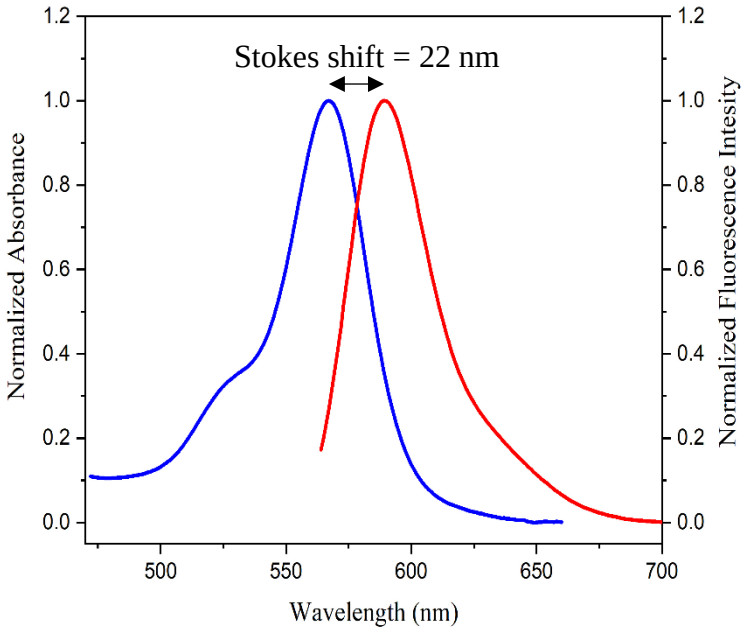

Figure S20. Normalized absorbance and fluorescence spectra of **Fe(RhoCat)$_3$** at pH 4.

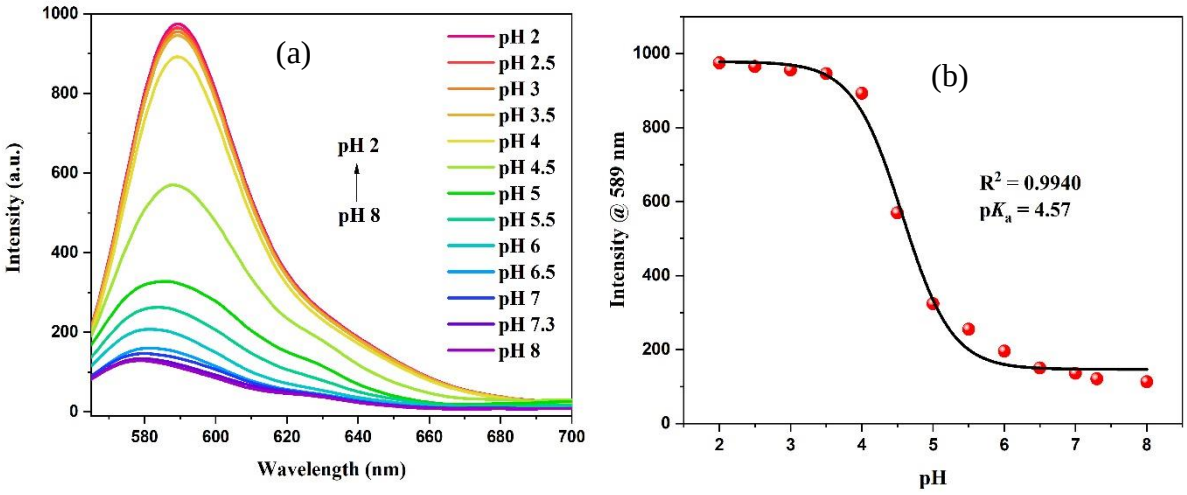

Figure S21. Fluorescence spectral change for **Fe(RhoCat)$_3$** (20 μM) versus pH variation in HEPES buffer (a). Plot of the fluorescence intensity at 589 nm as a function of pH.

Table S1. Selected bond lengths and bond angles calculated from DFT optimized structure

Bond angles (Å)				**Bond Angles (º)**	
Fe-O_1	2.080	Fe-O_2	2.042	O_1-Fe-O_2	79.1
Fe-O_3	2.096	Fe-O_4	2.039	O_3-Fe-O_4	79.1
Fe-O_5	2.080	Fe-O_6	2.038	O_5-Fe-O_6	79.0